The iron K line complex in NGC 1068: implications for X-ray reflection in the nucleus

K. Iwasawa[1], A.C. Fabian[1] and G. Matt[2]

[1] *Institute of Astronomy, Madingley Road, Cambridge CB3 0HA*
[2] *Dipartimento di Fisica, Universita di Roma III, Via della Vasca Navale 84, I-00146 Roma, Italy*

arXiv:astro-ph/9703159v1 25 Mar 1997

ABSTRACT
We report a new analysis of ASCA data on the iron K line complex in NGC 1068. The line complex basically consists of three components, as previously reported. A weak red wing of the 6.4 keV fluorescence iron K line is found. A plausible explanation is Compton scattering in optically thick, cold matter which can be identified with an obscuring torus or cold gas in the host galaxy. We also show that this 'Compton shoulder' should be observable with ASCA using a simulated reflection spectrum. In order to explain the two higher energy lines as well as the cold 6.4 keV line, we fit the ASCA data with a composite model of cold and warm reflection. This shows that cold reflection dominates the observed X-ray emission above 4 keV; the estimated scattering fraction from the warm medium is found to be ~ 0.08 per cent, an order of magnitude below the standard value of 1 per cent obtained from previous observations in other wavebands. The two higher energy lines have large equivalent width (~ 3 keV) with respect to the warm-scattered continuum, suggesting that efficient resonant scattering operates. The line energies are systematically lower than those expected from resonant lines for FeXXV and FeXXVI by ~ 100 eV. The redshifts may be due to either the ionized gas of the warm mirror receding at a radial velocity of 4000–5000 km s^{-1}, or effects of Compton scattering in a complicated geometry.

Key words: line: profiles – galaxies: active – galaxies: individual: NGC 1068 – X-rays: galaxies

1 INTRODUCTION

Since the discovery of the polarized broad line region (Antonucci & Miller 1985), the standard model for the Seyfert 2 galaxy NGC 1068 is of a Seyfert 1 nucleus hidden behind a thick obscuring torus. There is much observational support for this model (e.g., Antonucci 1993). Contrary to the powerful nuclear activity observed at some other wavelengths, the weakness of the observed X-ray luminosity and failure to detect any direct component, even up to 20 keV, strongly suggests that the direct X-ray radiation from the central source is blocked entirely from our direct view (Koyama et al 1989; Mulchaey et al 1995).

The lack of low energy absorption in the X-ray spectrum was interpreted as evidence that the observed X-rays are the scattered radiation of a hidden Seyfert 1 nucleus (e.g., Elvis & Lawrence 1988). However, extended soft X-ray emission (~ 13 kpc) is resolved with the ROSAT HRI (Wilson et al 1992), and an ASCA spectrum shows thermal emission, probably coming from the spatially extended circumnuclear starburst, dominates in the soft X-ray band (Ueno et al 1994). The ASCA spectrum then no longer looks

like a Seyfert 1, indicating very steep thermal emission below 3 keV (which now agrees with the Einstein Observatory IPC measurement by Monier & Halpern 1984) and only above 3 keV, where a flat continuum ($\Gamma \sim 1.2$) with strong iron K lines (Ueno et al 1994) is seen, is emission presumed to originate from the active nucleus.

Based on the unification model, a large equivalent width (EW) of the iron K line was predicted by Krolik & Kallman (1987). This was later verified by a Ginga observation ($EW \sim 1.3$ keV, Koyama et al 1989; Smith et al 1993). The line centroid energy of the iron K line was 6.55 ± 0.1 keV which suggested a blend of cold and ionized lines, but it could not be resolved at the spectral resolution of the Ginga LAC (Turner et al 1989). A subsequent BBXRT observation resolved the iron K line feature into three components for the first time (Marshall et al 1993). They were identified with cold Fe (less ionized than FeXVII at 6.4 keV), FeXXV and FeXXVI.

Several attempts to explain the iron K line feature have been made (Band et al 1991; Marshall et al 1994), assuming that all X-ray emission is scattered light from the active nucleus and the scattering medium is optically thin in order to

Table 1. Four gaussian fit to the iron K line complex. The line width of each component is assumed to be $\sigma = 10$ eV, since no significant broadnening ($\sigma < 80$ eV) is found. The EWs are with respect to the single power-law continuum with Galactic absorption (see text). Line-intensity ratios to the 6.4 keV line ($I/I_{6.4}$) are also shown.

| E | I | EW | $I/I_{6.4}$ |
keV	$10^{-5} \mathrm{ph\,s^{-1}\,cm^{-2}}$	keV	
6.21 ± 0.16	$0.51^{+0.70}_{-0.50}$	$0.11^{+0.15}_{-0.10}$	$0.10^{+0.13}_{-0.09}$
6.40 ± 0.03	$5.19^{+0.79}_{-1.27}$	$1.10^{+0.17}_{-0.27}$	1.00
6.61 ± 0.03	$3.20^{+1.00}_{-0.80}$	$0.69^{+0.22}_{-0.17}$	$0.62^{+0.23}_{-0.18}$
6.86 ± 0.05	$2.65^{+0.89}_{-0.87}$	$0.58^{+0.19}_{-0.19}$	$0.51^{+0.20}_{-0.20}$

account for the lack of low energy absorption. The observed continuum above 3 keV is unusually flat compared with that in Seyfert 1 galaxies observed with ASCA ($\Gamma \sim 1.9$; Nandra et al 1996; Reynolds 1996). Together with the presence of a strong 6.4 keV line, this instead suggests that reflection from cold, thick matter is an important component, as observed in other Seyfert 2 galaxies such as NGC 6552 (Fukazawa et al 1994) and the Circinus galaxy (Matt et al 1996a). To account for the three line components, Matt, Brandt & Fabian (1996) proposed a composite scenario in which two distinct reflections from an optically thick torus and an optically thin, warm scattering mirror together compose the observed X-ray spectrum of NGC 1068.

We report here the discovery of a Compton shoulder on the 6.4 keV fluorescence iron K line and a spectral analysis of the ASCA PV data based on the model by Matt et al (1996b). We assume the distance of NGC 1068 to be 22 Mpc throughout this paper.

2 THE ASCA DATA

NGC 1068 was observed on 1993 July 24 with ASCA (Tanaka, Inoue & Holt 1994) during the Performance Verification (PV) phase. Initial results have been published by Ueno et al (1994). We use only the Solid state Imaging Spectrometer (SIS; S0 and S1) data, because of their superior spectral resolution for resolving the iron K line complex. The source data of 38 ks are extracted from a circular region of a radius 3.2 arcmin, and the background data are taken from a source-free field in the same detector. Spectral fits are performed with the S0 and S1 data jointly while the figures presented are made by summing both detectors for display purposes. Errors on each spectral parameter are given at the 90 per cent confidence level for one interesting parameter.

2.1 Compton shoulder

We show the observed line profile of the iron K complex in Fig. 1. The underlying continuum is fitted with a single power-law model described below. Since X-ray emission below 3 keV is dominated by starburst emission (Ueno et al 1994) and there is evidence for emission lines due to Ar and Ca (see below) between 3 and 4 keV, we use the 4–10 keV data. Fitting the 4–10 keV data excluding the iron K line band 6–7 keV with a single power-law plus Galactic
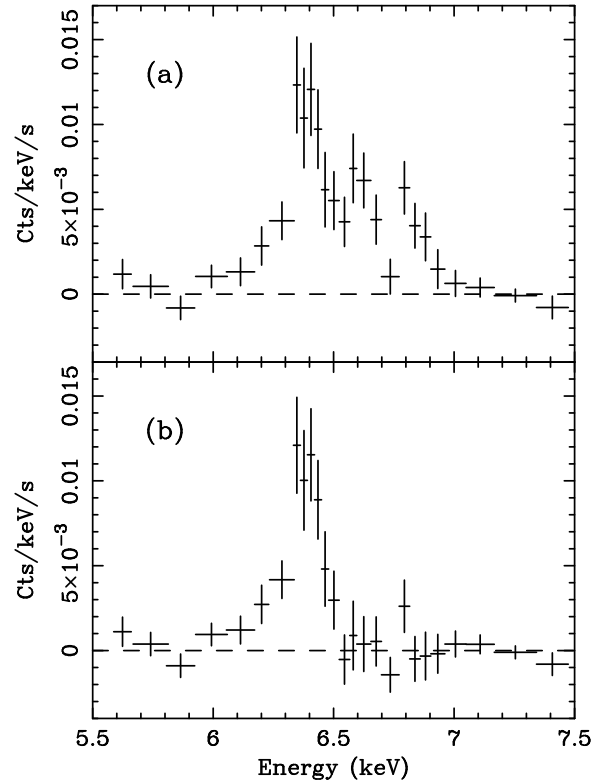

Figure 1. (*a*) Total line profile of the iron K line complex in NGC 1068 obtained from the ASCA SIS. The S0 and S1 are summed to display this figure. Note that the instrumental efficiency declines towards higher energy; e.g., the efficiency at 6.9 keV is 15 per cent lower than at 6.4 keV. (*b*) The two higher energy lines are subtracted from the total line profile. A clear line asymmetry is seen. The red wing can be identified with a Compton shoulder of the 6.4 keV line.

absorption $N_H = 4.5 \times 10^{20}$ cm^{-2} (Stark et al 1992), leaves the total line profile shown in Fig 1a. The photon-index is $\Gamma = 0.35^{+0.66}_{-0.30}$, flatter than that given in Ueno et al (1994) because of the exclusion of the 3–4 keV band where some emission lines are present, causing the slope to steepen.

As previously suggested by Marshall et al (1993) and Ueno et al (1994), three emission-line peaks are seen. These three lines do not show evidence for significant broadening ($\sigma < 80$ eV). However, there is a weak wing on the red side of the 6.4 keV line. To clarify this, we show only the 6.4 keV line profile in Fig. 1b, which was produced by fitting the two higher energy lines with a narrow ($\sigma = 10$ eV) gaussian and subtracting them from the total line profile. The subtraction of the two lines is fairly good as there are no significant residuals seen above 6.5 keV. The line profile is clearly more complicated than a single gaussian; the core emission is consistent with the SIS energy resolution, whereas a wing can be seen on the red side in contrast. Fitting the red wing by a gaussian gives a line energy of 6.21 ± 0.16 keV and an intensity one tenth of the 6.4 keV line with ~ 90 per cent confidence level. The four gaussians plus a power-law model now gives a good fit to the 4–10 keV data with $\chi^2 = 54.98$ for
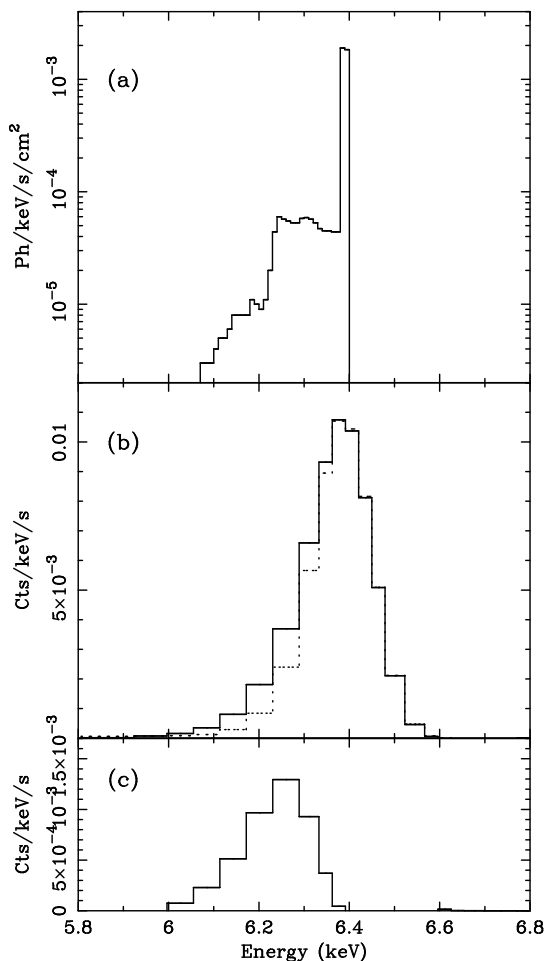
Figure 2. (a) Line profile of an iron K line from a Monte Carlo simulation of reflection in thick, cold matter (see text). To show the shape of the weak Compton shoulder, the intensity here has a logarithmic scale. (b) The line profile (solid line) folded through the SIS response from (a). A narrow ($\sigma = 10$ eV) gaussian with an intensity normalized to the peak intensity of the line core is also shown by the dotted line. Note that the spectral resolution of the SIS is FWHM ≈ 130 eV at 6.4 keV, appropriate for our data which were taken during the PV phase. (c) Difference between the line with the Compton shoulder and a narrow gaussian in (b). It is clear that the residual is observable with the SIS, consistent with the observed result.

70 degrees of freedom. The line energies, equivalent widths and relative line intensities of each line component are summarized in Table 1.

The possibility of a symmetric broad base to the 6.4 keV line cannot be excluded, since the subtraction of the higher energy lines will have eliminated any blue wing. A double gaussian, with a narrow and a broad component, fit to the 6.4 keV line profile is slightly worse than the one with the red wing (by $\Delta\chi^2 \simeq 1.4$), but acceptable. In this case, the line width of the broad component is $\sigma \sim 0.3$ keV.

Compton scattering is a likely mechanism to explain the red wing. A line extending only to lower energy indi-

cates that the electrons responsible for scattering are cold (Pozdnyakov, Sobol & Sunyaev 1979). Theoretical calculations of Compton reflection spectrum from optically thick, cold matter have already predicted such a weak red wing, the so called 'Compton shoulder' (George & Fabian 1991; Reynolds et al 1994), which is a characteristic feature due to Compton scattering of the 6.4 keV fluorescent line photons. It consists of a series of shoulders extending towards low energies. Computed line shapes due to the Compton scattering are presented in Hatchett & Weaver (1977); Pozdnyakov et al (1979); George & Fabian (1991); and Sunyaev & Churazov (1996). The first shoulder is due to single scattering and is spread over two Compton wavelengths ($\simeq 160$ eV); multiple scattering makes a further weak low energy tail.

If pure reflection from thick, cold matter is observed with ASCA, the Compton shoulder should be resolvable with the SIS. To demonstrate this we have used a Monte Carlo code kindly provided by C. Reynolds (see also George & Fabian 1991). The line profile derived from a Monte Carlo reflection spectrum with spectral resolution of 10 eV (Fig. 2a) is compared, after folding through the SIS response, with that of a narrow ($\sigma = 10$ eV) gaussian (Fig. 2b). The difference bewtween the two profiles should be detectable (Fig. 2c). The shape of the Compton shoulder depends slightly on geometry (e.g. Matt, Fabian & Reynolds 1996) and its height also depends on the abundance ratio of iron and the lighter elements, mainly oxygen, which absorb the 6.4 keV photons (George & Fabian 1991). In order that the shoulder is maximally broad, a large back-scattered component is required. The quality of the present data is not good enough for detailed spectral modelling, however, and we merely assume that reflection occurs from a face-on, semi-infinite slab with an optical depth of unity. The strength of the simulation has been adjusted to the observed intensity level. Although the residual profile due to the Compton shoulder shows some asymmetry, fitting this with a gaussian gives the line centroid energy ~ 6.24 keV and the intensity ratio to the gaussian line-core ~ 12 per cent. These values are in good agreement with the gaussian modelling of the observed line profile (see Table 1).

Note that the broad line from a relativistic accretion disk, such as that observed in Seyfert 1 galaxies (e.g., Tanaka et al 1995), is an unlikely explanation for the red wing, since we do not directly see the relativistic line emitting region (which emerges from within ~ 40 gravitational radii). A scattered relativistic line is also implausible. The scattering cone appears to have a half opening angle of $\sim 40°$ (Evans et al 1991; Tsvetanov et al 1996) and the inclination angle of the accretion disk in NGC1068 with respect to most of the scattering volume must therefore be near 40°. In this geometry the red wing of the diskline would be skewed down to 4 keV and peaked at energies well below 6 keV (see inclination angle dependence of diskline profiles in Fabian et al 1989) giving rise to a much broader red wing than observed.

2.2 Spectral fit with the composite model

The presence of the Compton shoulder indicates that reflection from optically thick cold matter is an important process in producing the observed hard X-ray emission in NGC1068. However, pure cold reflection alone does not explain the two higher energy lines.
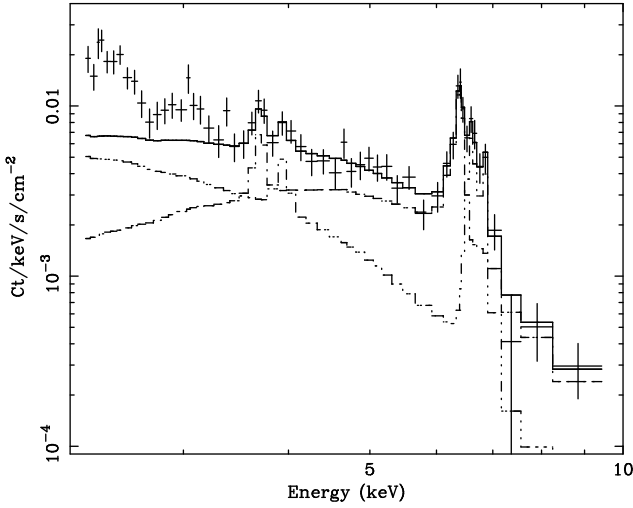
Figure 3. ASCA SIS spectrum of NGC 1068 fitted with the composite model. The best-fit model for the 3.2–10 keV band is shown as well as the cold reflection and warm scattered continuum plus ionized lines. The data below 3.2 keV down to 2.3 keV are also shown so that excess emission due to the starburst can be seen.
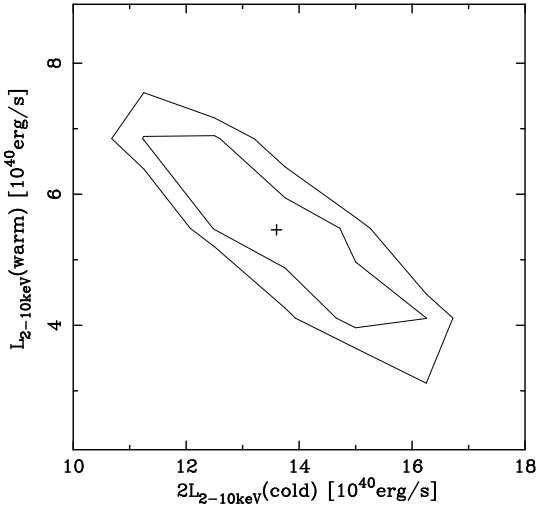

Figure 4. Contour plot of the 2–10 keV luminosities of the cold and the warm reflection continua obtained from the composite model fit. The luminosities are derived assuming the distance of NGC 1068 to be 22 Mpc. Note that the cold reflection luminosity is integrated over 2π (see text). Contours are drawn at 68 and 90 per cent confidence levels for two interesting parameters. The best-fit values, $2L_C = 1.36 \times 10^{41}$ erg s^{-1} and $L_W = 5.47 \times 10^{40}$ erg s^{-1}, are shown by a plus symbol.

Table 2. Equivalent widths of two calcium-K and three iron-K lines respect to each continuum conponent obtained from the composite model fit. EW_C and EW_W are equivalent widths respect to the cold reflection continuum and the power-law warm-reflection continuum, respectively. Note that the EW for the 6.4 keV line is the sum of the line-core and Compton shoulder.

E_{line} keV	EW_C keV	EW_W keV
3.71	$0.19^{+0.11}_{-0.11}$	—
3.94	—	$0.11^{+0.06}_{-0.10}$
6.40	$1.21^{+0.26}_{-0.28}$	—
6.61	—	$3.49^{+1.09}_{-0.87}$
6.86	—	$2.92^{+0.98}_{-0.96}$

It is likely that the higher energy lines are produced in optically thin ionized (warm) matter which is located above the obscuring torus and electron-scatters the continuum of the central source, as originally proposed by Krolik & Kallman (1987). If the ionized scattering medium is optically thin enough, photoelectric absorption has little effect on the electron-scattered continuum so the emergent spectrum retains almost all the original shape of the central source, in the ASCA band.

Thus, as proposed by Matt et al (1996b), a combination of cold and warm reflections could be a plausible description for the observed hard X-ray emission from NGC 1068. We therefore fit the ASCA spectrum with the composite model described above.

We assume that the incident spectrum of the central source is a power-law with $\Gamma = 2.0$, typical of Seyfert 1s (e.g., Nandra et al 1996; Reynolds 1996). The pure cold reflection continuum and the warm-scattered continuum are approximated by the viewing-angle averaged Lightman & White (1988) type reflection model and a power-law of $\Gamma = 2.0$ with no intrinsic absorption, respectively. The iron K line complex is modelled by four gaussians including the Compton shoulder. Weak line features due to calcium between 3.6–4 keV are also modelled by narrow gaussians. The 3.2–10 keV data are fitted with the composite model, and the best fit model gives $\chi^2 = 70.14$ for 83 degrees of freedom. The EW of each line are shown in Table 2. Note that the EW of the cold iron K line is the sum of the 6.4 keV line-core and the Compton shoulder measured with respect to the cold reflection continuum, and those of the two higher energy lines are with respect to the warm-scattered $\Gamma = 2.0$ power-law continuum.

Although only the 3.2–10 keV data are fitted, to show excess emission due to the starburst below the low energy bound, the 2.3–10 keV data are shown in Fig. 3. Two significant lines at 3.71 ± 0.04 keV and 3.94 ± 0.09 keV are identified with a neutral and helium-like calcium (CaXIX). The EW of the neutral Ca line with respect to the cold reflection continuum is $EW = 190 \pm 110$ eV, which is similar to that in NGC 6552 (Fukazawa et al 1994) but larger than that expected from a Monte Carlo simulation (~ 50 eV; Reynolds et al 1994). This is further evidence for cold reflection. Another line feature around 3.1 keV is due to $K\alpha$ emission from ArXVII which is probably from both the thermal emission and the warm scattering matter.

The 2–10 keV fluxes of the two components esti-

mated from the best-fit model are $F_X(\text{cold}) = 2.5 \times 10^{-12}\text{erg cm}^{-2}\text{ s}^{-1}$ for the cold reflection, and $F_X(\text{warm}) = 1.0 \times 10^{-12}\text{erg cm}^{-2}\text{ s}^{-1}$ for the warm scattered continuum. Confidence contours of the corresponding luminosities are given in Fig. 4, using a distance of 22 Mpc. The best-fit values in the 2–10 keV band are $6.8 \times 10^{40}\text{erg s}^{-1}$ for the cold reflection continuum and $5.5 \times 10^{40}\text{erg s}^{-1}$ for the warm reflection continuum, respectively. It should be noted that the luminosity is integrated over 2π for the cold reflection because of the assumed geometry whilst over 4π for the warm reflection. However, for a direct comparison of observed intensity between the two components, the cold reflection luminosity multiplied by 2 is shown in Fig. 4.

If significantly large absorption (say, $N_H > 10^{22}\text{cm}^{-2}$) or a starburst component is included in the fit, the value of L_W would be reduced slightly. Fitting the data in a higher energy band (e.g. 4–10 keV) gives poorer constraints on L_C and L_W. Results are consistent with those in Fig. 4, although the warm reflection component is not necessary at the 90 per cent confidence level.

3 DISCUSSION

3.1 Intrinsic luminosity

A rough estimate of the intrinsic X-ray luminosity can be obtained using the warm scattering luminosity $L_W \approx 5.5 \times 10^{40}\text{erg s}^{-1}$ derived from the composite model fit. For highly-ionized iron such as FeXXV and FeXXVI, resonant scattering plays an important role in making the EW large, if the scattering medium is optically thin (Band et al 1991; Matt et al 1996), but it is easily suppressed below the large observationally inferred values (Table 2) when the column density is, say, larger than 10^{22}cm^{-2} (e.g., see Matt et al 1996b). This indicates that the optical depth of the warm scattering mirror is small enough to allow efficient resonant scattering. Thus assuming a scattering depth ($nl\sigma_T$) of $0.002\tau_{0.002}$ so that the column density of the scattering mirror is $N_H \sim 3\times10^{21}\tau_{0.002}\text{cm}^{-2}$, and the fraction of the sky occupied by the scattering mirror, $0.25(\Omega/4\pi)_{0.25}$, the intrinsic luminosity is estimated to be $L' = L_W\tau^{-1}(\Omega/4\pi)^{-1} \simeq 1\times10^{44}\tau_{0.002}^{-1}(\Omega/4\pi)_{0.25}^{-1}\text{erg s}^{-1}$ in the 2–10 keV band, where the density and depth of the scattering medium are n and l, respectively, and L_W is the measured luminosity of the warm reflection continuum. This estimate is entirely independent of data in other wavebands.

There are further possible ways to estimate the intrinsic luminosity. Using the correlation between X-ray and [OIII]λ5007 luminosities ($\log L_{[\text{OIII}]}/\log L_{2-10\text{keV}} \sim -1.8$) derived by Mulchaey et al (1995), the 2–10 keV luminosity would be $L' \simeq 7 \times 10^{43}\text{erg s}^{-1}$. Note that the [OIII] flux was measured with a large aperture (10–15 arcsec, see Whittle 1992) containing the strong starburst region which could contribute some fraction of the flux. The estimate from the above, X-ray based, argument is consistent with this value. For a comparison, the far infrared luminosity measured with IRAS is $5 \times 10^{44}\text{erg s}^{-1}$ (e.g., David, Jones & Forman 1993), although this does contain a significant contribution from the circumnuclear starburst.

3.2 Reflection from cold matter

The detection of the Compton shoulder of the 6.4 keV iron fluorescent line is strong evidence that we are seeing reflection from optically thick, cold matter. The presence of the neutral calcium line supports this. The flat 4–10 keV continuum ($\Gamma \sim 0.4$) suggests that cold reflection is a major component of the observed X-ray emission from the active nucleus which dominates the observed radiation only in the energy band above 3 keV. In fact, the fit with the composite model of cold and warm reflections (Section 2.2) indicates that ~ 71 per cent of the total 2–10 keV flux comes from cold reflection.

Presumably the cold reflection occurs at the inner surface of the optically-thick, obscuring torus which entirely blocks the direct radiation from the central source in our direction (Ghisellini, Haardt & Matt 1993; Matt et al 1996b). For such a geometry only part of the reflection surface is visible to us. If that fraction is f_C, the observed luminosity is described as $L_C = f_C\eta L'$, where η is the total albedo of a cold reflector subtending a solid angle of 2π. Using values of $L_C = 6.8\times10^{40}\text{erg s}^{-1}$ (see Section 2.2 and Fig. 4), $\eta = 0.022$ (in the 2–10 keV band), and $L' = 7 \times 10^{43}L'_{43.8}\text{erg s}^{-1}$ (see Section 3.1), f_C is then found to be $\approx 4.4 \times 10^{-2}L'^{-1}_{43.8}$.

The small value for f_C suggests a high inclination of the obscuring torus (close to edge-on) if its inner surface is the reflecting source. Alternatively a torus of a small radial/axial ratio (Pier & Krolik 1993) is also possible, if it is not nearly edge-on. Recent water maser observations by Gallimore et al (1996) and Greenhill et al (1996) suggest a high inclination > 82 degrees of the maser disk which is on a pc scale with a toroidal geometry and is identified with the X-ray absorbing gas torus at large optical depth (i.e., $N_H > 10^{25}\text{cm}^{-2}$, Koyama et al 1989). A rather broad [OIII]λ5007 emission-line cone (projected opening angle $\theta_{\text{proj}} \sim 65$–$80°$, Cecil, Bland & Tully 1990; Evans et al 1991) also favours an edge-on torus over one with a large scale-height.

Another possible cold reflector is the cold gas in the bulge and disk of the host galaxy (Fabian 1977). Strong 6.4 keV line emission is observed from molecular clouds in our Galactic centre, where a strong iron K line emitter is Sgr B2, ~ 100 pc away from the Galactic centre. The X-ray spectrum there also shows a complex of iron K lines (Koyama et al 1996). As the stellar disk of NGC 1068 is almost face-on, contrary to the torus, radiation from the central source escaping from the torus can pass through some of the cold gas clouds in the host galaxy. The likely distances of cold clouds from the active nucleus and the disk-like geometry make the covering factor small, and consistent with the small f_C. If this is the case, future high spatial resolution mission like AXAF would resolve a conical shape to the iron K line emission.

The cold reflection spectrum has been studied by many authors (Guilbert & Rees 1988; Lightman & White 1988; George & Fabian 1991; Matt, Perola & Piro 1991; Reynolds et al 1994). The cold reflection-dominated spectrum in NGC 1068 predicts that a spectral break due to Compton down-scattering would be observed around 30 keV. This is consistent with the CGRO/OSSE upper limit and may be observable with high quality data from RXTE and SAX.

3.3   Reflection from warm matter

Cold reflection is a unique phenomenon at X-ray wavelengths. Warm scattering is much more relevant to the observed optical/UV scattering. The 2–10 keV luminosity of the warm-scattered continuum is $L_W \approx 5.5 \times 10^{40} \mathrm{erg\ s^{-1}}$, which implies a scattering fraction in the warm matter to be $f_W = L_W/L' \simeq 7.8 \times 10^{-4} L'^{-1}_{43.8}$. Various other observations of NGC 1068 suggest that the scattering fraction is approximately 1 per cent (summarized in Pier et al 1994). The X-ray scattering fraction appears to be an order of magnitude lower. Pier et al (1994) deduced the bolometric luminosity of NGC 1068 to be $\sim 7 \times 10^{44} f^{-1}_{0.01} \mathrm{erg\ s^{-1}}$, where the scattering fraction is $0.01\,f_{0.01}$. Since they assumed that the whole hard X-ray emission above 2 keV (as observed with BBXRT, Marshall et al 1993) is scattered by the warm mirror, contrary to our result, their estimate has been modified slightly.

If the two higher energy lines are due to FeXXV and FeXXVI, the ionization parameter of the warm scattering matter, $\xi = L'/nR^2$, is about several hundreds (Kallman & McCray 1982; Krolik & Kallman 1987; Band et al 1991), where R is a distance of the scattering medium from the central source. Assuming $l = R$, the column density can be written as $nl = L'(\xi l)^{-1}$. Since $f_W = \sigma_T nl(\Omega/4\pi)$,

$$l = \frac{\sigma_T L'^2}{\xi L_W}\left(\frac{\Omega}{4\pi}\right).$$

If $\xi = 600\,\xi_{600}$ and $\Omega/4\pi = 0.25(\Omega/4\pi)_{0.25}$ (e.g., Evans et al 1991) are taken, then the size of the scattering region is approximately $l \simeq 8\,\xi^{-1}_{600} L'^2_{43.8}(\Omega/4\pi)_{0.25}$ pc. This is large enough to be visible to us without occultation by a pc-scale torus; direct X-ray imaging of this is impossible at present as the angular size is the order of 0.1 arcsec (≈ 11 pc at D = 22 Mpc). The size of the optical/UV scattering nebula observed by spectropolarimetry with the Hubble Space Telescope (HST) is several tens pc or up to 200 pc (Antonucci et al 1994; Capetti et al 1995), the warm X-ray mirror is therefore smaller. The column density $nl = 5 \times 10^{21} L'^{-1}_{43.8}(\Omega/4\pi)_{0.25} \mathrm{cm^{-2}}$, which is small enough to allow efficient production of the resonant scattering lines of FeXXV and FeXXVI as mentioned in Section 3.1. To maintain the high value of ξ in order to emit the highly ionized iron lines over a large scale, a low mean electron density such as ~ 200 cm^{-3} is required.

3.4   Complexities

We have discussed X-ray scattering from a warm medium in the context of the standard unification model as proposed by Krolik & Kallman (1987) and Matt et al (1996b), i.e., the scattering medium is located outside the obscuring torus and is directly visible to us. However, there are some problems: (1) a very small scattering fraction $f_W \sim 0.8 \times 10^{-3}$; (2) disagreement of line energies discussed below; and (3) the location of the region where the higher energy lines are formed.

We note that the line energies for the two higher energy lines (6.61 keV and 6.86 keV) disagree with the energies of the resonant lines of FeXXV, 6.70 keV, and FeXXVI, 6.97 keV, (see Table 1) whilst that of the cold iron K line agrees with 6.40 keV perfectly. The shift of the line energies are

-90 ± 30 eV for FeXXV and -110 ± 50 eV for FeXXVI. We have checked that there are no significantly strong iron lines at the observed energies from any other ionization states (e.g., Beiersdorfer et al 1993). Interestingly, the shift of the two line energies are similar to each other ($\sim 1.5 \pm 0.6$ per cent lower than rest energies). If the redshift is due to the Doppler effect from receding warm scattering matter, then the radial velocity is ~ 4000–5000 km s^{-1}. The optical polarized broad Hβ line is also redshifted but only by 600 km s^{-1} (Antonucci & Miller 1985) from the narrow line component, which is explained as scattering in outflowing wind (Krolik & Begelman 1986; Balsara & Krolik 1993). As the discrepancy between the velocities is too large, the same outflowing wind is perhaps not an explanation. It should be noted however that the X-ray lines are produced in the mirror itself whilst the polarized broad line is scattered by the mirror.

The location of the gas emitting the two higher energy lines is an issue. It is supposed to lie outside the torus. Systematic studies of Seyfert 1 galaxies with ASCA show that a large fraction of them show evidence for partially ionized gas in the line of sight, implied by absorption edge feature mainly due to oxygen, OVII and OVIII (Reynolds 1996). A recent study of the warm absorber in MCG–6-30-15 (Otani et al 1996) suggests that the OVII and OVIII absorbers occupy distinct regions; the variability study locates the OVII absorber > 1 pc far from the central source, and the OVIII absorber in the broad-line region. If we observed this object from a different viewing angle, the OVII warm absorber would be seen as a scattering mirror. However, the ionization state implied from OVII ($\xi \leq$ a few tens erg cm s^{-1}) is too low for the emission of FeXXV and FeXXVI. If ionized gas in the nucleus of NGC 1068 has a similar ionization structure to that of MCG–6-30-15, the gas emitting the highly-ionized iron line should be located well within the torus like the OVIII absorber so that it would not be visible to us directly. If this is the case, the radiation emitted from the inner hot gas, including resonantly scattered FeXXV and FeXXVI lines, is also scattered into our line of sight by the cold reflecting matter. The line emission would be Compton scattered and then end up having line energies shifted lower as observed. Scattered continuum radiation would have the same shape as the cold reflection continuum.

We do however know that the optical/UV mirror (see e.g., Miller, Goodrich & Mathews 1991) is located outside the torus and is at least directly visible to us, so we should see some X-ray continuum scattered from it. (It is unlikely that this mirror is sufficiently ionized to produce the high ionization X-ray iron lines.) This may reconcile the small value of f_W. Importantly, the EW with respect to the warm reflection continuum, discussed before (e.g., Table 2, Sections 2.2 and 3.1), is now meaningless since the spatial origin of the lines and continuum is not the same. Uncertainties in the geometry of the inner nucleus and the mirrors make it difficult to estimate the expected luminosities from each component.

A further possibility, which can increase the predicted EW of the lines from highly ionized iron, is that there is velocity shear in the warm mirror. As discussed in Section 3.1, the EW decreases as the column density of the mirror increases as the line is absorbed. This assumes that the scattering medium is all at the same velocity. If, however there is

shear such that the velocity doppler-shifts the line by more than its spectral width (natural and thermal) over a typical mean free path, corresponding to a column of $\sim 10^{21} \mathrm{cm}^{-2}$, then much of the line is not resonantly absorbed in other parts of the mirror. A larger EW then arises from greater optical depths than assumed in Section 3.1 (see Fig. 9 in Matt et al 1996 for an indication of the effect). For a mirror gas temperature of about $10^6 \mathrm{K}$, the velocity shear needs to exceed about 50km s$^{-1}(10^{21}\,\mathrm{cm}^2)^{-1}$ for this to be significant. The upper limit on the width of the line (< 80 eV; Table 1) limits the extent of this effect. In this case the intrinsic luminosity can be less than we estimated in Section 3.1.

Higher resolution spectroscopy resolving the individual line shapes will test and discriminate between these hypothesis. Given the complex geometry and the possible complexities in the formation of the iron and other X-ray lines, we expect it to reveal that NGC 1068 has a rich and interesting spectrum.

ACKNOWLEDGEMENTS

REFERENCES

Antonucci R., Hurt T., Miller J. 1994, ApJ, 430, 210
Antonucci R.R.J., Miller J.S. 1985, ApJ, 297, 621
Antonucci R.R.J., 1993, ARAA, 31, 473
Balsara D.B., Krolik J.H., 1993, ApJ, 402, 109
Band D.L., Klein R.I., Castor J.I., Nash J.K., 1990, ApJ, 362, 90
Beiersdorfer P., Phillips T., Jacobs V.L., Hill K.W., Bitter M., von Goeler S., Kahn S.M., 1993, ApJ, 409, 846
Capetti A, Macchetto F., Axon D.J., Sparks W.B., Boksenberg A., 1995 ApJ, 452, L87
Cecil G., Bland J., Tully R.B., 1990, ApJ, 355, 70
David L.P., Jones C., Forman W., 1992, ApJ, 388, 82
Elvis M., Lawrence A., 1988, ApJ, 331, 161
Evans I.N., Ford H.C., Kinney A.L., Antonucci R.R.J., Armus L., Caganoff S., 1991, ApJ, 369, L27
Fabian A.C. 1977, Nat, 269, 672
Fukazawa Y. et al 1994, PASJ, 46, L141
Gallimore J.F., Baum S.A., O'Dea C.P., Brinks E., Pedlar A., 1996, ApJ, 462, 740
George I.M., Fabian A.C., 1991, MNRAS, 249, 352
Ghisellini G., Haadt F., Matt G., 1994, MNRAS, 267, 743
Greenhill L.J., Gwinn C.R., Antonucci R., Barcainis R., 1996, ApJ, 472, L21
Guilbert P.W., Rees M.J., 1988, MNRAS, 233, 475
Hatchett S., Weaver R., 1977, ApJ, 215, 285; erratum, 218, 931
Kallman T.R., McCray R. 1982, ApJS, 50, 263
Koyama K., Inoue H., Tanaka Y., Awaki H., Takano S., Ohashi T., Matsuoka M., 1989, PASJ, 41, 731
Koyama K., Maeda Y., Sonobe T., Takeshima T., Tanaka Y., Yamauchi S., 1996, PASJ, 48, 249
Krolik J.H., Begelman M.C., 1986, ApJ, 308, L55
Krolik J.H., Kallman 1987, ApJ, 320, L5

Krolik J.H., Madau P., Życki P.T., 1994 ApJ, 420
Lightman A.P., White T.R., 1988, ApJ, 335, 57
Marshall F.E., Netzer H., Arnaud K.A., Boldt E.A., Holt S.S., Jahoda K.M., Kelley R., Mushotzky R.F., 1993, ApJ, 405, 168
Matt G. et al, 1996a, MNRAS, 281, L69
Matt G., Fabian A.C., Reynolds C.S., 1996, MNRAS, submitted
Matt G., Fabian A.C., Brandt W.N., 1996b, MNRAS, 280, 823
Matt G., Perola G.C., Piro L., 1991, A&A, 247, 25
Miller J.S., Goodrich R.W., Mathews W.G., 1991 ApJ, 378, 47
Mulchaey J.S., Koratkar A., Ward M.J., Wilson A.S., Whittle M., Antonucci R.R.J., Kinney A.L., Hurt T., 1994, ApJ, 436, 586
Nandra K., George I.A., Mushotzky R.F., Turner T.J., Yaqoob T., 1996, ApJ, in press
Nandra K., Pounds K.A., 1994, MNRAS, 268, 405
Otani C., et al, 1996, PASJ, 48, 211
Pier E.A., Antonucci R., Hurt T., Kriss G., Krolik J., 1994, ApJ, 428, 124
Pier E.A., Krolik J.H., 1993, ApJ, 418, 673
Pozdnyakov L.A., Sobol I.M., Sunyaev R.A., 1979, A&A, 75, 214
Reynolds C.S., Fabian A.C., Makishima K., Fukazawa Y., Tamura T., 1994, MNRAS, 268, L55
Reynolds C.S., 1997, MNRAS, in press
Smith D.A., Done C., Pounds K.A., 1993, MNRAS, 263, 54
Stark A.A., Mammie C.F., Wilson R.W., Bally J., Linke R.A., Heiles C., Hurwitz M., 1992, ApJS, 79, 77
Sunyaev R., Churasov E., 1996, Pis'ma Astron. Zh., 22, 723
Tanaka Y. Inoue H., Holt S.S., 1994, PASJ, 46, L137
Tanaka Y., et al, 1995, Nat, 375, 659
Turner M.J.L. et al 1989, PASJ, 41, 345
Ueno S., Koyama K., Mushotzky R.F., Iwasawa K., Hayashi I., 1994, PASJ, 46, L7
Whittle M., 1992, ApJS, 79, 49
Wilson A.S., Elvis M., Lawrence A., Bland-Hawthorn J., 1992, ApJ, 391, L75